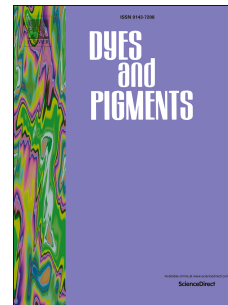


Accepted Manuscript

Concise design and synthesis of water-soluble fluorescence sensor for sequential detection of Zn(II) and picric acid *via* cascade mechanism

Kai Jiang, Si-Hong Chen, Shi-He Luo, Chu-Ming Pang, Xin-Yan Wu, Zhao-Yang Wang



PII: S0143-7208(19)30316-X

DOI: <https://doi.org/10.1016/j.dyepig.2019.04.023>

Reference: DYPI 7478

To appear in: *Dyes and Pigments*

Received Date: 10 February 2019

Revised Date: 17 March 2019

Accepted Date: 10 April 2019

Please cite this article as: Jiang K, Chen S-H, Luo S-H, Pang C-M, Wu X-Y, Wang Z-Y, Concise design and synthesis of water-soluble fluorescence sensor for sequential detection of Zn(II) and picric acid *via* cascade mechanism, *Dyes and Pigments* (2019), doi: <https://doi.org/10.1016/j.dyepig.2019.04.023>.

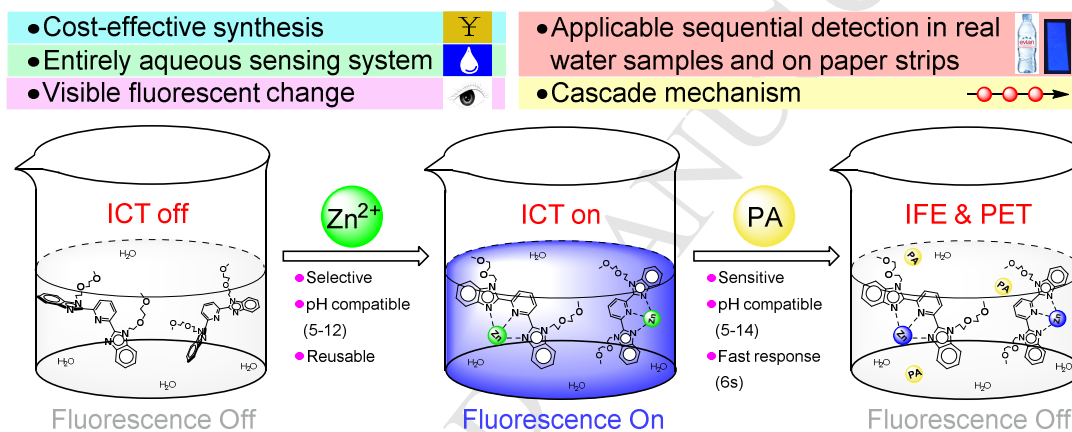
This is a PDF file of an unedited manuscript that has been accepted for publication. As a service to our customers we are providing this early version of the manuscript. The manuscript will undergo copyediting, typesetting, and review of the resulting proof before it is published in its final form. Please note that during the production process errors may be discovered which could affect the content, and all legal disclaimers that apply to the journal pertain.

Graphic Abstract

Concise design and synthesis of water-soluble fluorescence sensor for sequential detection of Zn(II) and picric acid via cascade mechanism

Author: Kai Jiang^{a,b,#}, Si-Hong Chen^{a,#}, Shi-He Luo^{a,b,*}, Chu-Ming Pang, Xin-Yan Wu,

Zhao-Yang Wang^{a,b,*}



Concise design and synthesis of water-soluble fluorescence sensor for sequential detection of Zn(II) and picric acid *via* cascade mechanism

Kai Jiang^{a,b,#}, Si-Hong Chen^{a,#}, Shi-He Luo^{a,b,*}, Chu-Ming Pang^a, Xin-Yan Wu^a, Zhao-Yang Wang^{a,b,*}

^a *School of Chemistry and Environment, South China Normal University; Key Laboratory of Theoretical Chemistry of Environment, Ministry of Education, Guangzhou 510006, China*

^b *Key Laboratory of Functional Molecular Engineering of Guangdong Province, South China University of Technology, 381 Wushan Road, Guangzhou 510640, China*

Kai Jiang and Si-Hong Chen contributed equally to this work.

*** Corresponding Author**

E-mail: wangzy@scnu.edu.cn. Tel: 8620-39310258.

E-mail: pinky_r@163.com.

Abstract

Under microwave assistance, 2,6-bis(benzimidazolyl)-pyridine has been concisely synthesized and further productively converted to the functional molecule **BMBP** via accessible *N*-alkylation reaction. For the introduction of alkoxyalkyl chain, this original substance **BMBP** with better solubility in water exhibits specific fluorescence response toward Zn^{2+} from colourless to blue in aqueous solution. A sequential detection for picric acid (PA) can be conducted in this following system, showing the high selectivity and sensitivity of quenching over other analogues. On the basis of the comparison with the control **BMBB**, a cascade sensing mechanism has been disclosed to accelerate the recognition of structure-property relationship, which is fully supported by LC-MS, ^1H NMR, lifetime measurement and theoretical calculation. Noteworthy, **BMBP** is also readily available for practical application not only in quantitative determination of Zn^{2+} and PA in real water samples, but also in visible detection of two analytes in multiple forms on paper test strips, offering convenient process for low-cost, portable and versatile sensing device.

Keywords

Water-soluble sensor; Sequential detection; Cascade mechanism; Test strips

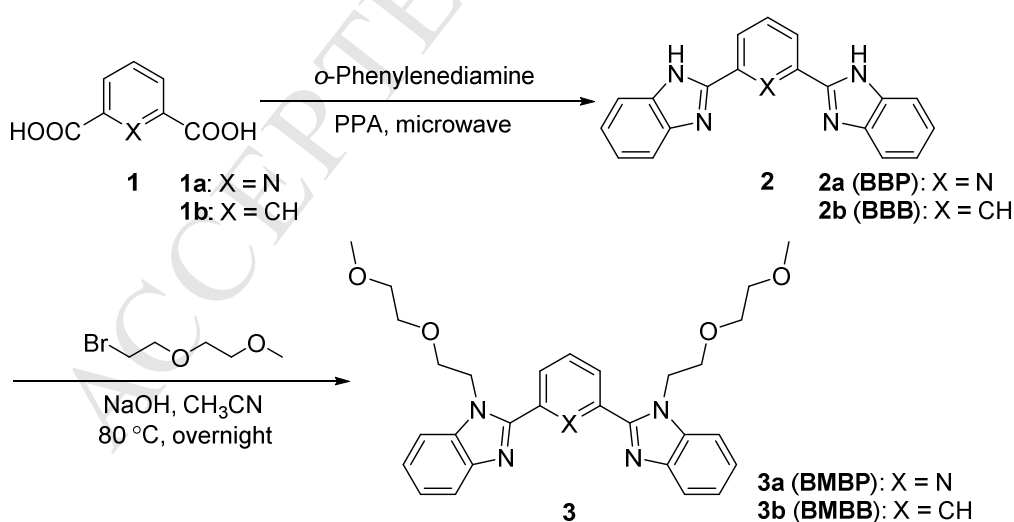
1. Introduction

As the second abundant transition metal in the human body, Zn^{2+} assumes an irreplaceable role in numbers of physiological processes such as enzymatic catalysis, structural organization, and functional regulation [1]. However, the anomalous concentration of Zn^{2+} may not only cause neurogenic disease, but also bring about contamination to soil as well as water [2, 3]. Due to many merits of fluorescence sensing technique, such as high sensitivity, instant response and operational simplicity, a plethora of fluorescence sensors with good performance on monitoring Zn^{2+} have been reported in recent years [2, 4-7]. Even so, some drawbacks like water insolubility, complicated synthesis or inferior selectivity, have still limited the application of the existing Zn^{2+} sensors [8-11]. Therefore, it will be greatly valuable for practicality to exploit fluorescence sensor that can efficiently detect Zn^{2+} in aqueous solution.

Knowing as the highly explosive property, picric acid (PA) is also a prevalent sensing object as well as TNT. Notably, PA is of certain water solubility and toxicity in lower concentration, which may induce intense stimulation and health problem related to eye, skin and respiratory after contact with its vapour, powder or dilute solution [12-14]. In light of implementing the rapid and handy sensing of PA, fluorescence sensors become highly desirable in this field [15-22]. In fact, most of the reported fluorescence PA sensors possess good selectivity and sensitivity [18-20, 23-25], but some of them remain improvement owing to the high cost, slow response and dependence of organic solvents [26-29]. Hence, the development of environmentally comparable fluorescence sensor for on-site detection of PA in water samples is under pressing concern.

2,6-bis(benzimidazolyl)-pyridine (**BBP**) is always served as ligand coordinating with Cu^{2+} , Rh^{3+} , Rh^{4+} , etc., because of its structural characteristics on multiple binding sites and coordination

cavity [30-32]. Meanwhile, the outstanding emission property of benzimidazole moiety in **BBP** is extensively applied in fluorescence sensors [33-35]. Herein, we selected **BBP** as the skeleton of the fluorescence sensor, and searched for a reformative synthetic way to acquire good yield at the same time. Utilizing the active N-H on imidazole for chemical modification, two hydrophilic alkyloxy groups have been introduced to this skeleton to overcome the poor water solubility of **BBP**, giving the target molecule **BMBP** as expected fluorescent probe (**Scheme 1**). It is revealed that **BMBP** shows highly selective fluorescence response toward Zn^{2+} in entirely aqueous solution, and the mixture of **BMBP** and Zn^{2+} can further detect PA by fluorescence quenching. These enable **BMBP** to be developed as a promising fluorescence sensor for sequential detection of Zn^{2+} and PA not merely in real water samples, but also on the paper test strips. In addition, the control compound **BMBB** with a similar structure to **BMBP** have also been obtained through the same route (**Scheme 1**) to investigate the sensing mechanism.



Scheme 1. Synthetic route for target compound **BMBP** and control compound **BMBB**.

2. Experimental section

2.1. Chemicals and apparatus

Melting point was performed on an X-5 digital melting point apparatus without correcting. Low resolution electrospray ionization mass spectra (ESI-MS) were recorded on Thermo LCQ DECA XP MAX mass spectrometer or Agilent Technologies 6120, while the high resolution mass spectra (HRMS) were recorded on Bruker maXis impact. ^1H and ^{13}C NMR spectra were collected on BRUKER DRX-600 spectrometer using TMS as an internal standard. Elemental analysis was obtained with Perkin Elmer Series II 2400. UV-vis spectra were measured by using a Shimadzu UV-2700 ultraviolet absorption detector at room temperature. The fluorescence spectra were recorded with a Hitachi F-4600 spectrophotometer at room temperature; and the slit width was 5 nm for both excitation and emission. The pH values were measured by a PHS-25C meter. Fluorescence lifetime was measured by FLS 920 fluorescence spectrometer. All chemicals used within this work were of analytical grade purity. For the real water samples, tap water was collected from laboratory; pond water and river water were collected from South China Normal University and the Pearl River after centrifugation.

2.2. Synthesis

2.2.1. Synthesis of compound intermediate 2

Based on our previous report in terms of the microwave-assisted method for the synthesis of benzimidazole compound [36], we conducted the synthesis of the intermediate **2** in a household microwave oven. Acid **1** (1.5 mmol), 1,2-diaminobenzene (3.3 mmol) and 25 mL polyphosphoric acid (PPA) were added into a 50 mL round bottom flask. The mixture was intermittently irradiated

in a microwave cavity with an output at 40 % (320 W) for specified times (30 s per irradiation). After that, the reaction was stopped by adding water, and the mixture was regulated to the pH range of 9-10 with sodium hydroxide, and a dark green solid was obtained by an immediate filtration. At last, the crude product was recrystallized by ethanol to give the intermediate **2**.

2,6-Bisbenzimidazolylpyridine (**2a**, **BBP**), white solid, m.p. > 310 °C, Yield 48.5 % (46.0 % in literature [37]); ¹H NMR (DMSO-*d*₆-TMS, 600 MHz): δ = 7.27-7.33 (2H, m, ArH), 7.34-7.41 (2H, m, ArH), 7.75 (2H, d, *J* = 6.0 Hz, ArH), 7.79 (2H, d, *J* = 6.0 Hz, ArH), 8.19 (1H, t, *J* = 6.0 Hz, PyH), 8.35 (2H, d, *J* = 6.0 Hz, PyH), 13.02 (2H, s, NH); ¹³C NMR (DMSO-*d*₆, 150 MHz): δ = 112.3, 120.2, 121.8, 122.7, 124.2, 134.8, 139.7, 144.6, 148.2, 150.9; ESI-MS, *m/z* (%): Calcd for C₁₉H₁₂N₅⁺ ([M-H]⁺): 310.12 (100), Found: 310.46 (100); Anal. Calcd for C₁₉H₁₃N₅: C 73.30, H 4.21, N 22.49, Found: C 73.41, H 4.23, N 22.36.

1,3-Bisbenzimidazolylbenzene (**2b**, **BBB**), white solid, m.p. 305.1-305.7 °C, yield 46.8 % (87.0 % in literature [38]); ¹H NMR (DMSO-*d*₆, 600 MHz): δ = 7.19-7.30 (4H, m, ArH), 7.57 (2H, d, *J* = 6.0 Hz, ArH), 7.71 (2H, d, *J* = 6.0 Hz, ArH), 7.75 (1H, t, *J* = 6.0 Hz, ArH), 8.27 (2H, d, *J* = 6.0 Hz, ArH), 9.06 (2H, s, ArH), 13.12 (2H, s, NH).

2.2.2. Synthesis of compound **3**

According to the literature [39], we followed the N-alkylation reaction to carry out the synthesis of compound **3**. A 100 mL round bottom flask was charged with intermediate **2** (1 mmol), 1-bromo-2-(2-methoxyethoxy)ethane (2.2 mmol) and sodium hydroxide (4 mmol) in acetonitrile (15 mL). The reaction mixture was stirred at 80 °C overnight. After removing the solvent, the residue was dissolved in dichloromethane. The organic solution was washed with water three times

and then dried over anhydrous magnesium sulfate. Purified by column chromatography on silica gel with gradient eluents of petroleum ether and ethyl acetate, the pure target compound **3** was afforded.

2,6-Bis(1-(2-(2-methoxyethoxy)ethyl)-2,6-bisbenzimidazolyl)pyridine (**3a**, **BMBP**), colourless oily liquid, yield 43.2 %; ^1H NMR (CDCl_3 , 600 MHz): δ = 3.16 (6H, s, OCH_3), 3.20 (4H, t, J = 6.0 Hz, OCH_2), 3.30 (4H, t, J = 6.0 Hz, OCH_2), 3.75 (4H, t, J = 6.0 Hz, OCH_2), 4.94 (4H, t, J = 6.0 Hz, NCH_2), 7.31-7.40 (4H, m, ArH), 7.55 (2H, d, J = 6.0 Hz, ArH), 7.87 (2H, d, J = 6.0 Hz, ArH), 8.07 (1H, t, J = 6.0 Hz, PyH), 8.34 (2H, d, J = 6.0 Hz, PyH); ^{13}C NMR (CDCl_3 , 150 MHz): δ = 44.6, 58.8, 69.7, 70.4, 71.7, 107.8, 110.8, 120.1, 123.0, 123.7, 125.7, 136.4, 138.2, 142.4, 149.7, 150.3; ESI-MS, m/z (%): Calcd for $\text{C}_{29}\text{H}_{34}\text{N}_5\text{O}_4^+$ ($[\text{M}+\text{H}]^+$): 517.25 (100), Found: 516.85 (100); Anal. Calcd for $\text{C}_{29}\text{H}_{33}\text{N}_5\text{O}_4$: C 67.55, H 6.45, N 13.58, Found: C 67.63, H 6.41, N 13.47.

1,3-Bis(1-(2-(2-methoxyethoxy)ethyl)-1H-benzimidazol-2-yl)benzene (**3b**, **BMBB**), colourless oily liquid, yield 47.5 %; ^1H NMR (CDCl_3 , 600 MHz): δ = 3.22 (6H, s, CH_3), 3.39 (4H, t, J = 6.0 Hz, OCH_2), 3.51 (4H, t, J = 6.0 Hz, OCH_2), 3.90 (4H, t, J = 6.0 Hz, OCH_2), 4.51 (4H, t, J = 6.0 Hz, NCH_2), 7.32-7.37 (4H, m, ArH), 7.51-7.55 (2H, m, ArH), 7.70 (1H, t, J = 6.0 Hz, ArH), 7.82-7.88 (2H, m, ArH), 8.02 (2H, d, J = 6.0 Hz, ArH), 8.28 (1H, s, ArH); ^{13}C NMR (CDCl_3 , 150 MHz): δ = 45.0, 58.9, 69.3, 70.7, 71.8, 110.5, 120.0, 122.7, 123.0, 125.1, 129.1, 131.2, 135.2, 135.8, 143.0, 153.4; ESI-MS, m/z (%): Calcd for $\text{C}_{30}\text{H}_{34}\text{N}_4\text{O}_4^+$ ($[\text{M}+\text{H}]^+$): 515.26 (100), Found: 514.90 (100); Anal. Calcd for $\text{C}_{30}\text{H}_{33}\text{N}_4\text{O}_4$: C 70.02, H 6.66, N 10.89, Found: C 70.03, H 6.63, N 10.94.

2.3. Methods

2.3.1. General procedure for optical spectral measurements

The compound **3** were dissolved in THF to acquire 10 mM stock solution. Then, the 10 μM

aqueous solution of compound **3** was prepared for the measurements of both UV-*vis* absorption and fluorescence spectra under room temperature. Both the excitation and emission slit widths were set at 5 nm during the fluorescence experiments.

2.3.2. Limit of detection

According to the literature [40, 41], the limit of detection (LOD) was determined by using equation: $LOD = 3\delta/K$. Herein, δ is the standard deviation of the blank measurements ($n = 10$), and the K is the slope of the calibration curve.

2.3.3. Calculation of Stern-Volmer constant

According to the literature [24, 41], the Stern-Volmer quenching constant (K_{sv}) was calculated according to the Stern-Volmer equation: $I_0/I = K_{sv}[Q] + 1$, where I_0 and I are the fluorescence intensities observed in the absence and presence of PA, respectively; $[Q]$ is the quencher concentration.

Caution! PA, 2,4-DNP, and NP used in the present study are highly explosive and should be handled only in small quantities.

3. Results and discussion

3.1. Design and synthesis of target molecule **BMBP**

The existence of the multiple nitrogen atoms and semi-enclosed structure [30, 42, 43] in **BBP** offer it significant binding affinity to metal ions, while the benzimidazole groups [33-36, 44] in

BBP provide it excellent fluorescence behaviour. For these reasons, the basic skeleton of **BBP** was chosen as the donator and fluorophore of the fluorescence sensor for metal ion. Thus, **BBP** as an intermediate was concisely synthesized *via* an improved approach within an hour by the aid of microwave technology.

To improve the water solubility of the sensor and make it more practical, two hydrophilic alkoxy groups were considered to chemically combine with **BBP** on the reactive imidazole N-H where the substitution reaction can be easily carried out. Indeed, as designed, the successfully obtained compound **BMBP** has largely improved water solubility and expectable sensing performance, which will be confirmed in the following discussions.

Meanwhile, we also synthesized the control compound **BMBB** *via* the same synthetic route (**Scheme 1**) to support the building strategy and sensing mechanism of **BMBP**. Both of the novel compounds **BMBP** and **BMBB** were systematically characterized by ^1H , ^{13}C NMR, ESI-MS (the corresponding spectra, **Figs. S1-S10**, see **Supplementary Material**) and elemental analysis, and the obtained data were consistent with the anticipation.

3.2. Fluorescence sensing of Zn^{2+}

At the beginning, we investigated the water solubility of **BMBP** by comparing the UV-*vis* absorption spectra with **BBP**. After 0.1 mmol of these two compounds were respectively deposited in 1 L water, the 10^{-4} M solutions were acquired with adequate dissolution. As shown in **Fig. S11**, a clear absorption band at 310 nm belongs to **BMBP**, while obviously no absorption band can be observed for **BBP**. The absolutely larger absorbance of **BMBP** indicates the significant enhancement of water solubility of **BMBP** versus **BBP**, which can be ascribed to the contribution of

the hydrophilic alkoxy chains.

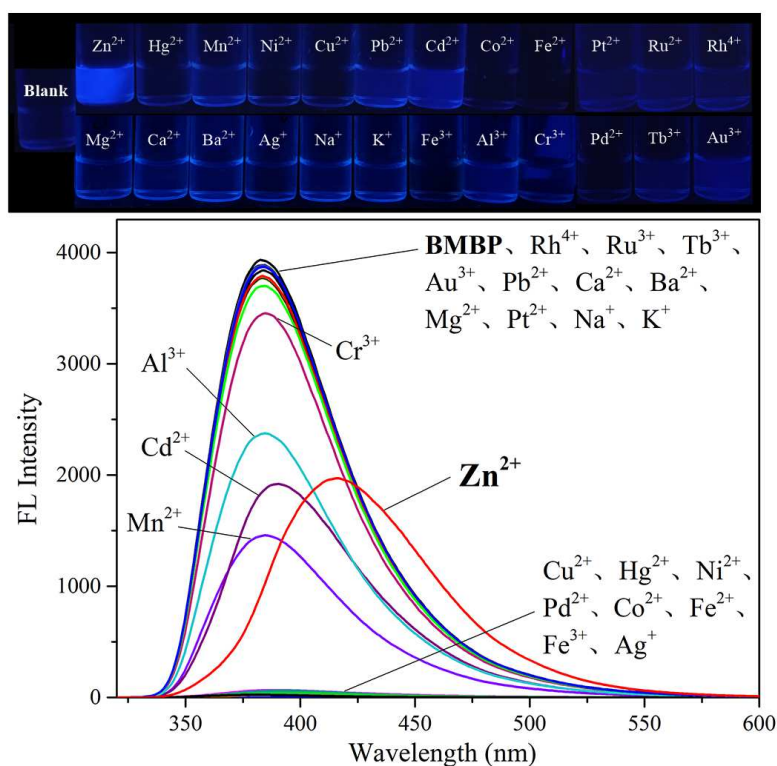


Fig. 1. Fluorescence spectra of compound **BMBP** (10^{-4} M in water, $\lambda_{\text{ex}} = 310$ nm) with different metal ions (5 equiv.) dissolved in water. Inset: visible fluorescent change of compound **BMBP** (10^{-4} M in water) with various metal ions (5 equiv.) under 365 nm UV lamp.

Subsequently, we investigated the selectivity of the fluorescence sensing studies of **BMBP** solution (10^{-4} M in water) towards 24 different metal ions, i.e. Na⁺, K⁺, Ag⁺, Zn²⁺, Fe²⁺, Pd²⁺, Ca²⁺, Ba²⁺, Mg²⁺, Pt²⁺, Cd²⁺, Pb²⁺, Mn²⁺, Cu²⁺, Hg²⁺, Ni²⁺, Co²⁺, Al³⁺, Cr³⁺, Fe³⁺, Ru³⁺, Tb³⁺, Au³⁺, Rh⁴⁺. As depicted in **Fig. 1**, the **BMBP** exhibits the sole emission peak at 383 nm upon 310 nm excitation, and the fluorescence is colourless under 365 nm UV light as the emission wavelength locates at nearly ultraviolet region. After adding 5 equiv. of these 24 metal ions into **BMBP** solution

respectively, a distinct red shift of the emission peak to visible region can be observed only for Zn^{2+} , while there is no obvious shift occurrence for the other metal ions. By viewing under 365 nm UV light, the addition of Zn^{2+} causes the clear fluorescence change of **BMBP** solution from colourless to blue, while the others give slight changes as the emission wavelength is still beyond the visible region (**Fig. 1, inset**). The unique “off-on” fluorescent response towards Zn^{2+} implies the potential of **BMBP** being a highly selective fluorescence sensor for Zn^{2+} over other metal ions in water *via* either fluorescence spectroscopic analysis or naked-eye inspection. Besides, the control compound **BMBB** was also proceeded with the selectivity studies, whereas none of the metal ions in **BMBB** (10^{-4} M in water) solution can cause conspicuous shift of the emission peak including Zn^{2+} (**Fig. 2**). The weak interaction between **BMBB** and Zn^{2+} is supposed to be the reason for this phenomenon.

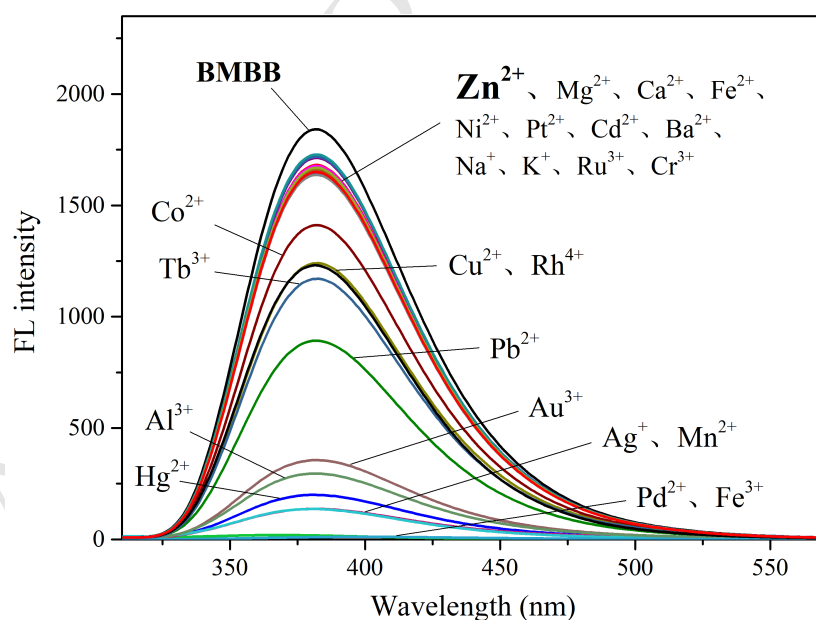


Fig. 2. Fluorescence spectra of control compound **BMBB** (10^{-4} M in water, $\lambda_{\text{ex}} = 310$ nm) with different metal ions (5 equiv.) dissolved in water.

The fluorometric titration experiment of **BMBP** ($10\ \mu\text{M}$) was then carried out with Zn^{2+} in water. As shown in **Fig. 3**, the initial emission peak at 383 nm gradually shifts to 415 nm upon the incremental addition of Zn^{2+} , and this bathochromic shift is almost terminated at 5 equiv. of Zn^{2+} . To inspect the relationship between the amount of Zn^{2+} and the wavelength of maximum emission, we integrated these two groups of data and built up a bi-exponentially fitted curve in good correlation ($R^2 = 0.992$) as depicted in the inset of **Fig. 3**. Moreover, the LOD for the Zn^{2+} is calculated to be $1.83 \times 10^{-7}\ \text{M}$ (11.97 ppb) by virtue of the partial linear fitted data (**Fig. S12**). This value of LOD is superior to many other Zn^{2+} sensors [8, 9, 45-48] (For more examples, please see **Table S1**, the comparison of **BMBP** with other Zn^{2+} sensors in **Supplementary Material**), which indicates that **BMBP** can sensitively monitor Zn^{2+} in water.

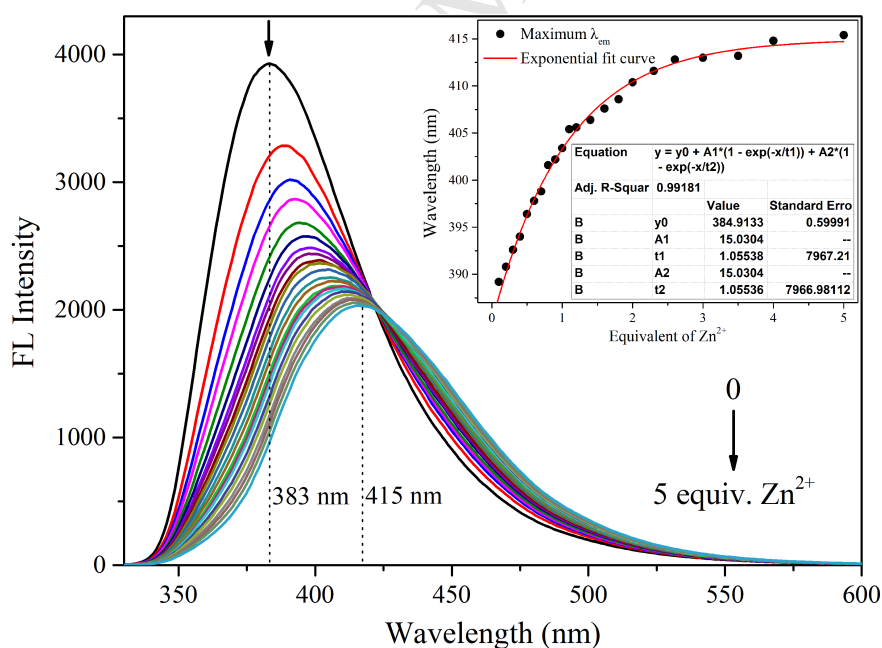


Fig. 3. Fluorescence spectra of compound **BMBP** ($10^{-4}\ \text{M}$ in water) upon the addition of Zn^{2+} dissolved in water ($\lambda_{\text{ex}} = 310\ \text{nm}$); Inset: the functional relationship between the maximum λ_{em} and equivalents of Zn^{2+} .

Since the response time is a vital parameter for metal ions sensor, we measured the time-dependent Zn^{2+} detection by recording the instantaneous fluorescence intensity of **BMBP** at 415 nm. As shown in **Fig. S13**, the fluorescence intensity decreases rapidly within few seconds after the addition of 5 equiv. of Zn^{2+} into the **BMBP** solution (10^{-4} M in water), and finally keeps constant in the next 4 min, whereupon the fluorescence response of **BMBP** sensing Zn^{2+} can be concluded to approximately 4 min.

The tolerability of pH is also essential to survey for the fluorescence sensor applied in solution [49]. Herein, we marked down the maximum fluorescence intensity of the **BMBP** (10^{-4} M) in aqueous system with different pH values from 1 to 14 before and after introduction of 5 equiv. Zn^{2+} . It can be learnt from **Fig. S14** that when the pH is below 5, the intensity is strongly declined whether there is or not Zn^{2+} in **BMBP** solution. When the pH reaches to 5-12, the intensity as well as the case when sensing Zn^{2+} may be backed to the normal. When the pH is over 12, the original intensity is still normal as before but remains unchanged after the addition of Zn^{2+} . These results denote that the suitable pH values of the aqueous system for **BMBP** sensing Zn^{2+} range from 5 to 12, which is broader than many other Zn^{2+} sensors [9, 48, 50-54].

3.3. Sequential sensing of PA

For a good sensor, to implement the sequential detection means to not only reduce the cost of making sensor, but also improve the sensing efficiency [55, 56]. Thus, many sensor with sequential sensing performance on bis- or multi-analytes received particular attention in recent years [57-59]. Generally, these sensors may respond to multiple ions [60-63] or small molecules [64], even some of them can sequentially detect ion to molecule [65-67]. In view of knowing the “off-on”

fluorescent response towards Zn^{2+} , we conjectured that **BMBP** might be further employed to visualize the sequential detection of PA after Zn^{2+} within the same aqueous system. Therefore, the following PA sensing experiments have been observed.

To validate if the **BMBP** can sequentially monitor PA after Zn^{2+} , the **BMBP-Zn²⁺** solution stemming from the foregoing experiments of Zn^{2+} detection was then coped with the selectivity studies of PA among a bunch of analogues, including nitroaromatic compounds (DNP, TNT, NP, etc., their corresponding structures are presented in **Fig. S15**) and other interferents (HBAc, Phenol). With the same condition, 2 equiv. PA and the other analogues were respectively added into **BMBP-Zn²⁺** to perform the fluorescence assay. As described in **Fig. 4**, the introduction of PA induces significant fluorescence quenching of **BMBP-Zn²⁺** from blue to colourless, and the quenching efficiency reaches to 84.3 %. On the other hand, the same amount of DNP and NP only brings to 48.6 % and 36.2 % quenching efficiency, which cannot lead to the distinguishable fluorescence change as PA. This can be attributed to the more favorable electrostatic interaction between **BMBP-Zn²⁺** and PA permitted by the more electron-deficient property of PA. This interaction may further facilitate the photoinduced electron transfer (PET) process to deliver the remarkable quenching of **BMBP-Zn²⁺** selectively toward PA [16, 22, 68]. In addition, the other nitro compounds show negligible impact to the fluorescence of **BMBP-Zn²⁺**. We have also investigated the selectivity towards 10 different anions commonly in water. As anticipated, these anions cannot produce any obvious changes to the fluorescence spectra of **BMBP-Zn²⁺** (**Fig. S16**). Thus, the above observations prove that **BMBP-Zn²⁺** can serve to selectively detect PA in water through a visible “on-off” fluorescence signal.

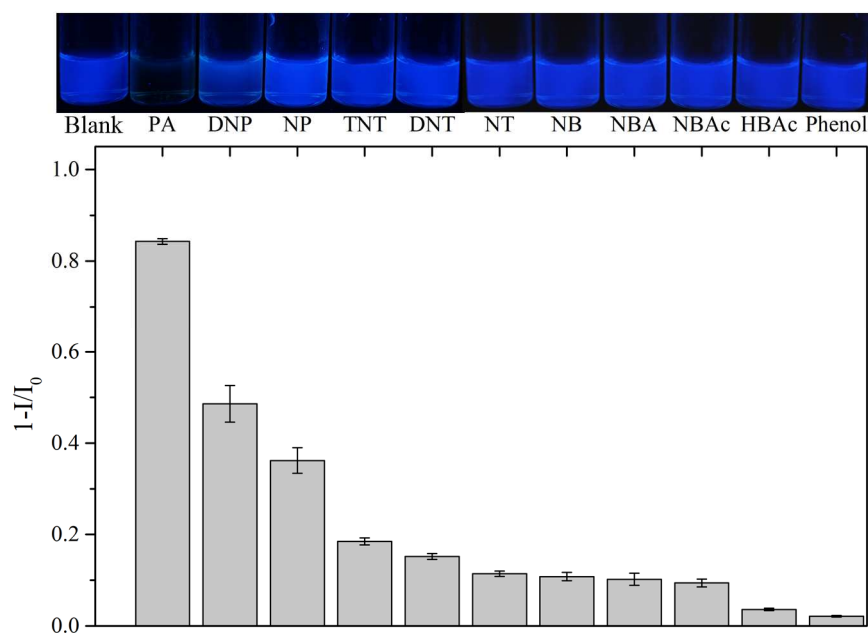


Fig. 4. Comparison of fluorescence quenching efficiency and visible fluorescent colour changes under 365 nm UV light of **BMBP-Zn²⁺** after interaction with 2 equiv. PA or other analogues respectively.

We further investigated the fluorometric titration of PA to analyze the sensing behaviour. As elucidated in **Fig. 5**, with the addition of PA from 0 to 4 equiv., the fluorescence intensity of **BMBP-Zn²⁺** at 415 nm is gradually descended. The fluorescence quenching efficiency reaches to 99.5 % after dropping with 4 equiv. PA into **BMBP-Zn²⁺**. To place the fluorescence intensity and the equivalent of PA together, an exponential curve with 0.997 of R^2 can be fitted, which offers the possibility of **BMBP-Zn²⁺** for quantitative PA determination. The LOD is calculated to be 2.16×10^{-7} M (49.49 ppb) from the fitted linear equation of converted titration data (**Fig. S17**). This value of the LOD possesses certain advantage among the reported PA sensors [26-29, 69-73], which reflects the good sensitivity of **BMBP-Zn²⁺** towards PA in water (For more examples, please see

Table S2, the comparison of **BMBP-Zn²⁺** with other PA sensors in **Supplementary Material**).

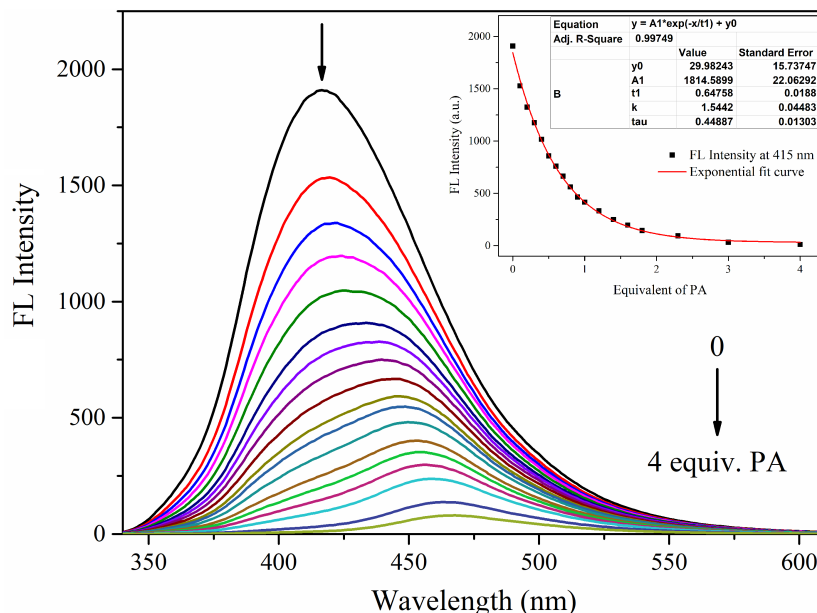


Fig. 5. Fluorescence spectra of **BMBP-Zn²⁺** upon the addition of different equivalents of PA dissolved in water ($\lambda_{\text{ex}} = 310 \text{ nm}$); Inset: the functional correlation between fluorescence intensity at 415 nm and equivalent of PA.

To further evaluate the quenching efficiency, the fluorometric titration data were transformed to the Stern-Volmer plot showing in **Fig. S18**. The plots show upward linearity at a lower concentration of PA ($0-0.7 \times 10^{-4} \text{ M}$), and the quenching constant (K_{sv}) is therefore calculated to be $2.72 \times 10^4 \text{ M}^{-1}$. This value is higher than some reported PA sensor [70-73], which further demonstrates the sensitive detection of **BMBP-Zn²⁺** toward PA. In addition, a steep curve can be viewed at a higher concentration of PA, which is presumably due to the existence of superamplified quenching effect [18].

The response time of sensing PA was also investigated by scanning the time-dependent

fluorescence intensity of **BMBP-Zn²⁺** at 415 nm. Once 4 equiv. PA is added into the **BMBP-Zn²⁺** system, the fluorescence intensity sharply goes down in few seconds and turns to stable after 6 s (**Fig. S19**). This quick response enables **BMBP-Zn²⁺** to be an on-site fluorescence sensor for PA detection in aqueous solution, which is faster than many reported PA sensors [27, 70, 71, 74].

To test the stability of sensing PA, we further recorded the fluorescence intensity of **BMBP-Zn²⁺** at 415 nm varying different pH values from 1 to 14 before and after adding with PA (**Fig. S20**). Similar with the behaviour of Zn²⁺ detection, the emission intensity of **BMBP-Zn²⁺** is insusceptible to the solution with pH values in 5-14. And within this range, the quenching efficiency can also be kept over 95 %. Thus, **BMBP-Zn²⁺** is confirmed to be pH-tolerable to monitor PA in water above plenty of reported PA sensors [13, 21, 41, 72, 74].

3.4. Sensing mechanism

To ascertain the sensing mechanism of **BMBP** towards Zn²⁺, the UV-*vis* absorption spectra of **BMBP** with Zn²⁺ in water have been carried out at first (**Fig. S21**). It can be learnt that **BMBP** may witness a decrease of absorbance at 310 nm along with an emergence of new absorbance at around 345 nm. This new absorbance may derive from the formation of **BMBP-Zn²⁺** complex instead of the absorbance of Zn²⁺ as known by the absorption spectrum for only 5 equiv. Zn²⁺ (blue line in **Fig. S21**). What's more, the existence of **BMBP-Zn²⁺** complex was further confirmed by HRMS. The sample for measurement was collected from the Zn²⁺ sensing experiment after dilution by water, and the results were shown in **Fig. 6**. Clearly, three dominant peaks have been captured. The one at *m/z* 516.2160 is assigned to [**BMBP** + H]⁺ along with the nearby [**BMBP** + Na]⁺. The other one at *m/z* 624.1796 is assigned to [**BMBP** + Zn²⁺ + C₂H₅O⁻]⁺, which can be the symbol of 1:1 interaction

between **BMBP** and Zn^{2+} in the sensing system. Referring to the reported method [54], the binding constant (K_a) of **BMBP-Zn** $^{2+}$ is calculated to be $4.88 \times 10^4 \text{ M}^{-1}$ according to a Benesi-Hildebrand plot (**Fig. S22**). On the contrary, there isn't any possible peak for **BMBB-Zn** $^{2+}$ that can be found in the HRMS of **BMBB** with Zn^{2+} (**Fig. S23**). As a coherent conclusion with selectivity assay, this possibly points to the weak interaction between **BMBB** and Zn^{2+} .

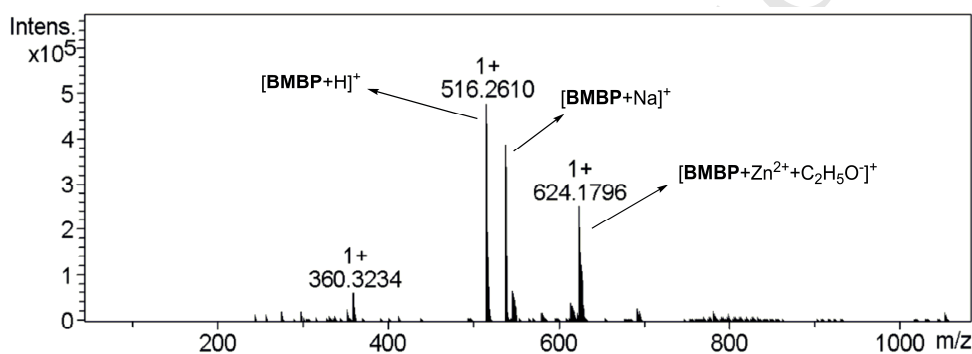


Fig. 6. HRMS spectrum of Zn^{2+} sensing system.

To unveil the interaction pattern of **BMBP** with Zn^{2+} and PA in solution, we have made a parallel comparison of the partial ^1H NMR spectra before and after their interaction in mixed solvent of $\text{THF-}d_6$ and D_2O (**Fig. 7**). It is not difficult to find that there is a downshift for the chemical shift of the whole aromatic hydrogen after the addition of Zn^{2+} , especially the largest shift for H_b from 8.02 to 8.14. This implies that Zn^{2+} may strongly bind to **BMBP** and the N atom on pyridine is likely to be one of the binding sites. Moreover, the H_c has the larger downshift (7.68 to 7.75) than H_d (7.54 to 7.60), suggesting that the unalkylated N atom in imidazole ring may participate in binding while the alkylated N atom doesn't. However, the further addition of 2 equiv.

PA seems not bring any shift of the aromatic H, which indicates the absence of specific interaction between **BMBP** and PA. To our surprise, the comparative analysis on ^1H NMR spectra using control **BMBB** (Fig. S24) shows that, there is a downshift for most aromatic H except for H_i after the addition of 5 equiv. Zn^{2+} , and the downshift of H_c (7.68 to 7.80) is larger than that of H_b (7.60 to 7.65). These indicate the fact that **BMBB** may also interact with Zn^{2+} by combination on imidazole N atom, but the binding mode is certainly different with **BMBP-Zn}^{2+}. This difference in binding mode between **BMBB** and Zn^{2+} may not bring to the effect of the extended conjugate as well as **BMBP**, which is confirmed by the later theoretical calculation.**

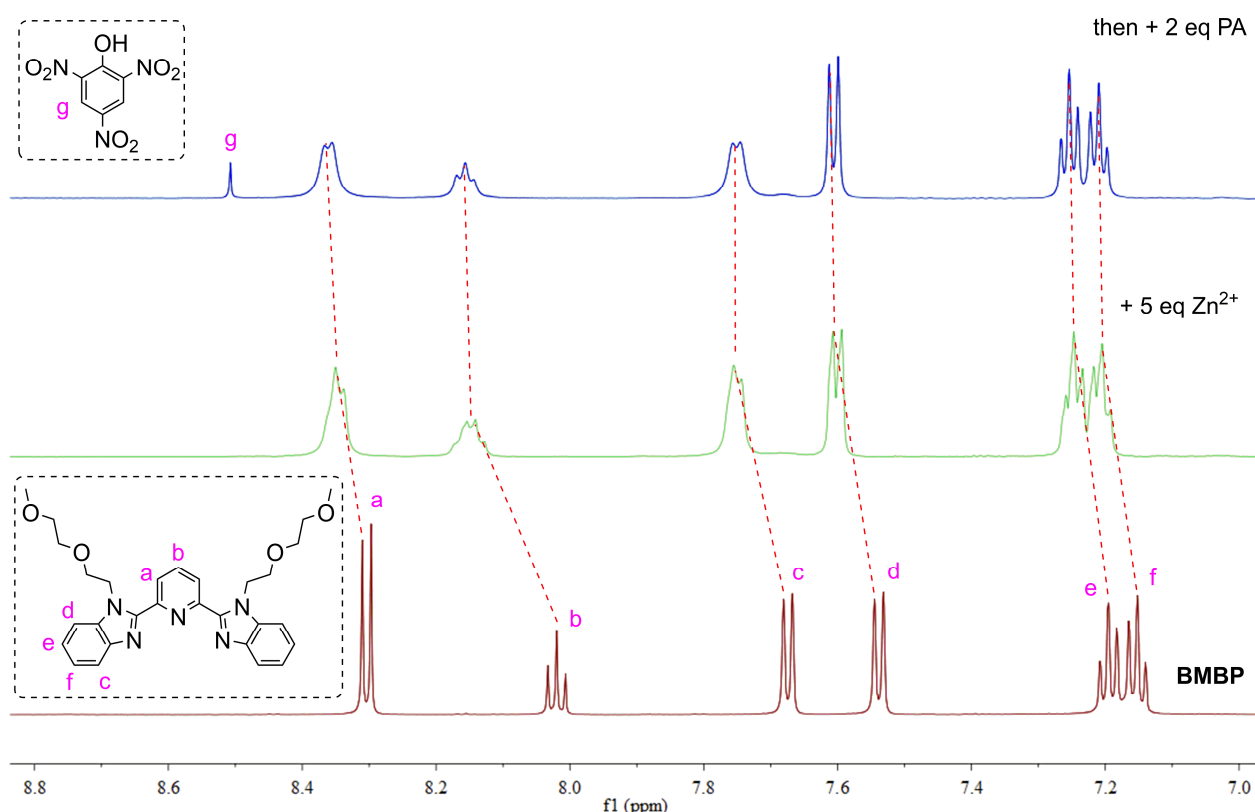


Fig. 7. Partial ^1H NMR spectra (8.8-7.0 ppm region) of **BMBP** (10^{-4} M in $\text{THF-}d_8$ and D_2O) before and after the sequential addition of Zn^{2+} and PA.

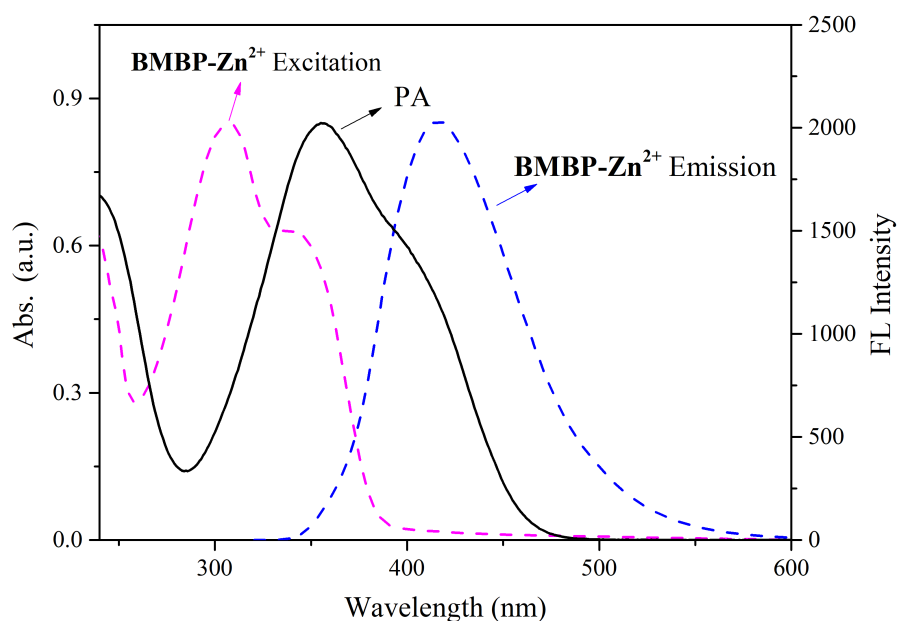


Fig. 8. Spectral overlap between UV-vis absorption spectra of PA, excitation and emission spectra of **BMBP-Zn²⁺**.

Aiming to gain in insight into the quenching mechanism of sensing PA in water, the absorption spectrum of PA is merged with the excitation and emission spectra of **BMBP-Zn²⁺** as description in **Fig. 8**. Not only a large area of overlap appears between the absorption spectrum of PA and the excitation spectrum of **BMBP-Zn²⁺**, but also a middle area of overlap between the absorption spectrum of PA and the emission spectrum of **BMBP-Zn²⁺** can be observed. Based on this observation, it is assumed that both the inner filter effect (IFE) and Förster resonance energy transfer (FRET) are probably responsible for the fluorescence quenching [75-77]. We also investigated the spectral overlap for the other tested PA analogues (**Fig. S25**). Likewise, DNP and NP exhibit partial overlap with the excitation or emission spectra of **BMBP-Zn²⁺**, but the other tested nitro compounds do not. This indicates that the IFE or FRET effect may occur after

BMBP-Zn²⁺ interacting with PA, DNP and NP, while the other nitro compounds cannot. Noticeably, it is a fact that DNP and NP containing less nitro groups show smaller quenching efficiency than PA as shown in **Fig. 4**. This potentially releases a signal that a synergistic mechanism in addition to IFE or FRET may contribute to selective fluorescence quenching of **BMBP-Zn²⁺** with respect to PA over other tested PA analogues.

To further verify the major reason for quenching induced by PA, the lifetime of **BMBP** was subsequently measured in the absence and presence of PA preceded by Zn²⁺. As shown in **Fig. S26**, the time-correlated single photon counting (TCSPC) plots of **BMBP**, **BMBP-Zn²⁺** and **BMBP-Zn²⁺** with PA show almost complete overlap. And their lifetimes calculated from the single-exponentially fitted TCSPC plots are almost the same also (**Table 1**). These represent that the possibility of FRET effect should be ruled out and the IFE should be one of the major effects during the quenching process [75-77].

Table 1. Fluorescence lifetime data for **BMBP** with various analytes.

Substance in solution	τ (ns)	χ^2
BMBP	2.88	1.006
BMBP + 5 eq Zn ²⁺	2.90	1.019
BMBP-Zn²⁺ + 1 eq PA	2.86	1.105
BMBP-Zn²⁺ + 2 eq PA	2.87	1.043

To better understand the mechanism of fluorescence response, according to the reported method [5, 78], we performed the theoretical research by employing the density functional theory

(DFT) in Gaussian 09. B3LYP/6-31g* basis set. Especially, water was chosen as the solvent for the structural optimization of **BMBP**, **BMBP-Zn²⁺**, and PA. The results are shown as **Fig. 9**. The calculated HOMO-LUMO energy levels and their energy gaps (ΔE) of **BMBP**, **BMBP-Zn²⁺**, and PA are summarized in **Fig. 9a**. Based on the results of HRMS spectrum and ¹H NMR studies, a reasonable structure for **BMBP-Zn²⁺** has been optimized and presented in **Fig. 9b**.

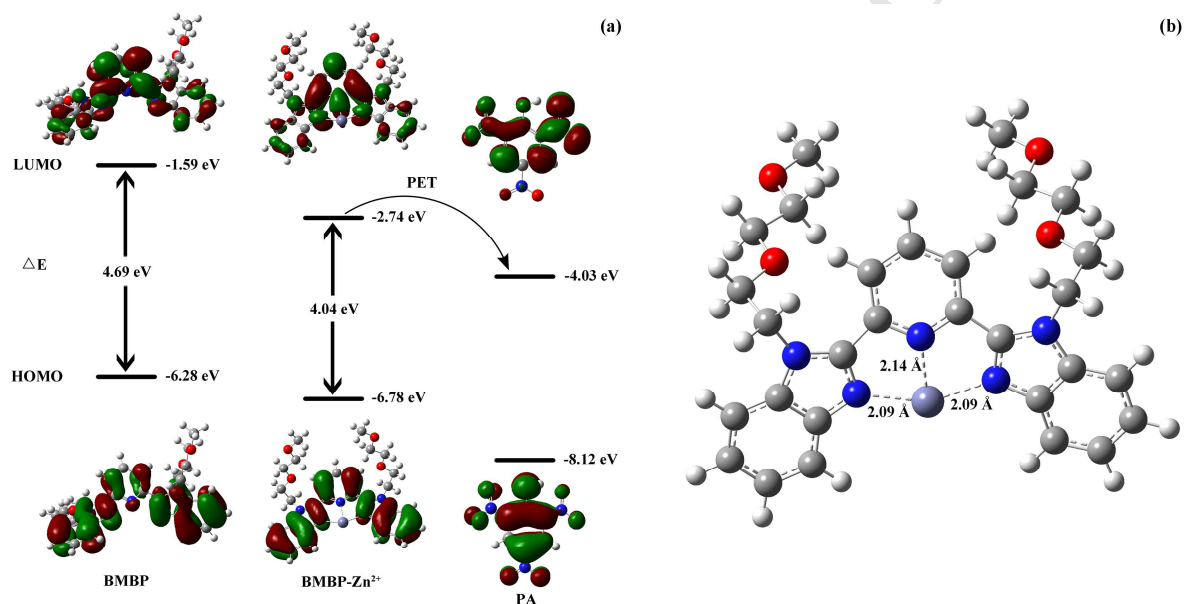


Fig. 9. (a) HOMO-LUMOs of **BMBP**, **BMBP-Zn²⁺** and PA calculated by the DFT methods; (b) Optimized structure of **BMBP-Zn²⁺** and length of partial bonds.

Initially, the simulation of **BMBP** displays a distort morphology in water owing to the rotation of benzimidazole moieties. After binding with Zn²⁺, the planarity of **BMBP** has been drastically promoted and the LUMO of **BMBP** massively transfers from benzimidazole moieties to pyridine ring, which indicates the activation of intramolecular charge transfer (ICT) process leading to the

fluorescent red shift [40, 79]. Moreover, the ΔE for **BMBP-Zn²⁺** is smaller than **BMBP**, which can also explain the red shift of fluorescence resulting in the “off-on” response for sensing Zn²⁺ [40, 80]. In addition, we also finished the calculation and simulation of **BMBB** with Zn²⁺ (**Fig. S27**). The decrease value of ΔE for **BMBB** after binding with Zn²⁺ is 0.2 eV (**Fig. S27a**), which is much more smaller than 0.65 eV of **BMBP** (**Fig. 9a**). Perhaps, for the steric hindrance of Ar-H, the distance of Zn to N atoms in **BMBB** is shown to be longer than that in **BMBP-Zn²⁺**, and the middle benzene in the optimized structure of **BMBB-Zn²⁺** is nonplanar with the benzimidazole groups (**Fig. S27b**). These differences between **BMBB** and **BMBP** may possibly indicate the less likely activation of ICT process for **BMBB-Zn²⁺** and further account to the irresponsive fluorescence of **BMBB** towards Zn²⁺.

The aforementioned PET process is suggested to be one of the quenching mechanisms. We can directly get the proof from comparing the orbital energy of **BMBP-Zn²⁺** and PA [16, 81]. It should be noted from **Fig. 9a** that the LUMO energy of electron-deficient PA is higher than the HOMO energy of **BMBP-Zn²⁺** but lower than the LUMO energy of **BMBP-Zn²⁺**, allowing the facile PET process from the LUMO of the excited **BMBP-Zn²⁺** to the LUMO of PA as non-radiative decay [81, 82]. For the other tested nitro compounds, their LUMO energy levels are higher than PA (**Fig. S28**), which indicates their less driving force of PET process and the highest electron-transfer efficiency from **BMBP-Zn²⁺** to PA. This also demonstrates the selective fluorescence quenching response of **BMBP-Zn²⁺** towards PA.

Consequently, a convinced cascade sensing mechanism with a suggested interaction mode for the sequential fluorescence detection of Zn²⁺ to PA was presented in **Fig. 10** according to the above investigations. Upon the addition of Zn²⁺ in **BMBP** aqueous solution, the ICT effect was switched

on by the restricted rotation of benzimidazole moieties and the extension of molecular planarity after 1:1 coordination, leading to the visible “off-on” fluorescent response. The sequential addition of PA into the following system causes significant “on-off” fluorescence change *via* a synergistic effect of IFE and PET. To make an overview of this sensing process, we can conclude that a cascade mechanism of “ICT-IFE&PET” occurs with the visible “off-on-off” fluorescent response in sequential detection of Zn^{2+} and PA in water.

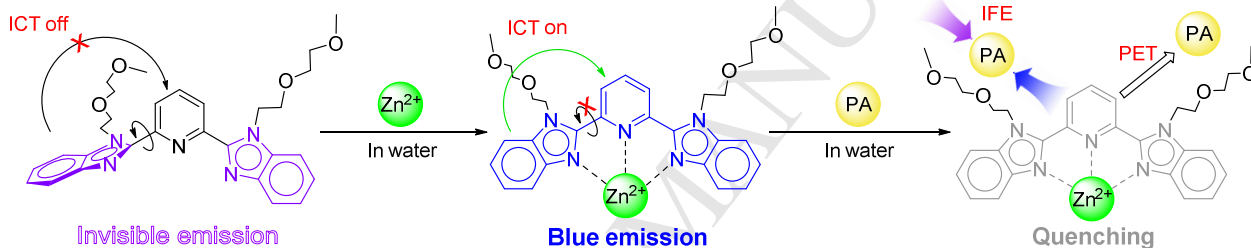


Fig. 10. Proposed cascade sensing mechanism of compound **BMBP** towards Zn^{2+} and PA.

3.5. Reversible detection of Zn^{2+}

The reversibility is widely recognized as an important nature of sensors [39, 83]. According to the reference [7], we introduced EDTA to perform the reversible test of **BMBP** sensing Zn^{2+} . As illustrated in **Fig. 11**, the maximum λ_{em} can back to the initial 383 nm from 415 nm after a certain amount of EDTA adding into **BMBP-Zn²⁺** in water, and the fluorescent colour correspondingly backs to invisible from blue within the first cycle. Such behaviour can be maintained in 5 cycles, which encourages **BMBP** to be a reusable fluorescence sensor for Zn^{2+} detection in water [7, 84].

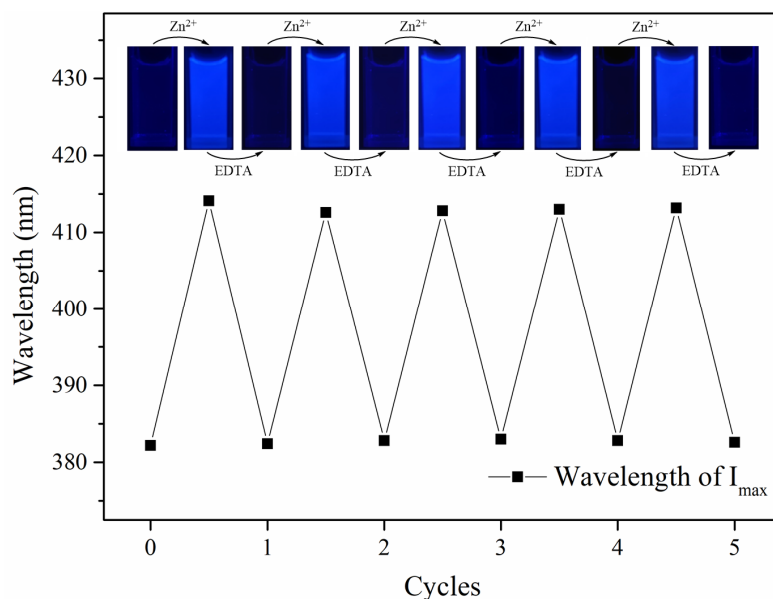


Fig. 11. Reversible changes in the maximum λ_{em} of **BMBP** (10^{-4} M in water) upon the alternate addition of Zn^{2+} and EDTA.

3.6. Application in real water samples

Attempt to develop the application of **BMBP** in real water samples, tap water, pond water and river water were prepared for the tested **BMBP** solution. For the procedure [52, 53], different amounts of Zn^{2+} were added into the as-prepared **BMBP** solution. The readout of their maximum λ_{em} was processed to the theoretical value by putting into the bi-exponentially fitted curve in **Fig. 3**, and then compared with the actual value to output the recoveries. Similarly, the readout of fluorescence intensity after sequential addition of PA was put into the exponentially fitted curve in **Fig. 5**. Each group of water samples was carried out for three independent tests to afford the Relative Standard Deviation (RSD). The results were summarized in **Table 2**. It can be seen that, the recovery for Zn^{2+} is 100 ± 2.3 %, while for PA is 100 ± 5.9 %. This indicates that the theoretical

value of either Zn^{2+} or PA is found to be largely aligned with the actual value in the three tested water samples. Moreover, the repeatability ($RSD \leq 6.2\%$) is also satisfactory [85]. Thus, it is confirmed that **BMBP** has the potency to sequentially and quantitatively detect Zn^{2+} and PA in real water samples.

Table 2. Sequential detection of **BMBP** towards Zn^{2+} and PA in real water samples.

Samples	Zn^{2+} added (10^{-4} M)	Zn^{2+} found (10^{-4} M)	Recovery (%)	RSD (%)	PA added (10^{-4} M)	PA found (10^{-4} M)	Recovery (%)	RSD (%)
Tap water	2.34	2.39	102.1	4.6	1.52	1.49	98.0	2.7
Pond water	0.87	0.85	97.7	2.6	3.26	3.25	99.7	1.8
River water	1.91	1.94	101.6	5.1	0.34	0.36	105.9	6.2

3.7. Paper strips for sequential detection

In consideration of developing convenient, economical and efficient sensing materials, we fabricated the **BMBP**-coated fluorescent paper strips for the investigation as the reported procedure [15, 67]. To investigate the sensing performance of the **BMBP**-coated paper strip, we dropped the Zn^{2+} solution on it and tested with fluorescence spectra. Shown as the line **a** and **b** in **Fig. 12(1)**, the **BMBP**-coated paper strip dealt with Zn^{2+} shows red-shifted emission which is kept in consistency with the foregoing experiments in water. Furthermore, its fluorescent colour changes from colourless to blue towards Zn^{2+} , which is shown as **Fig. 12(2)**.

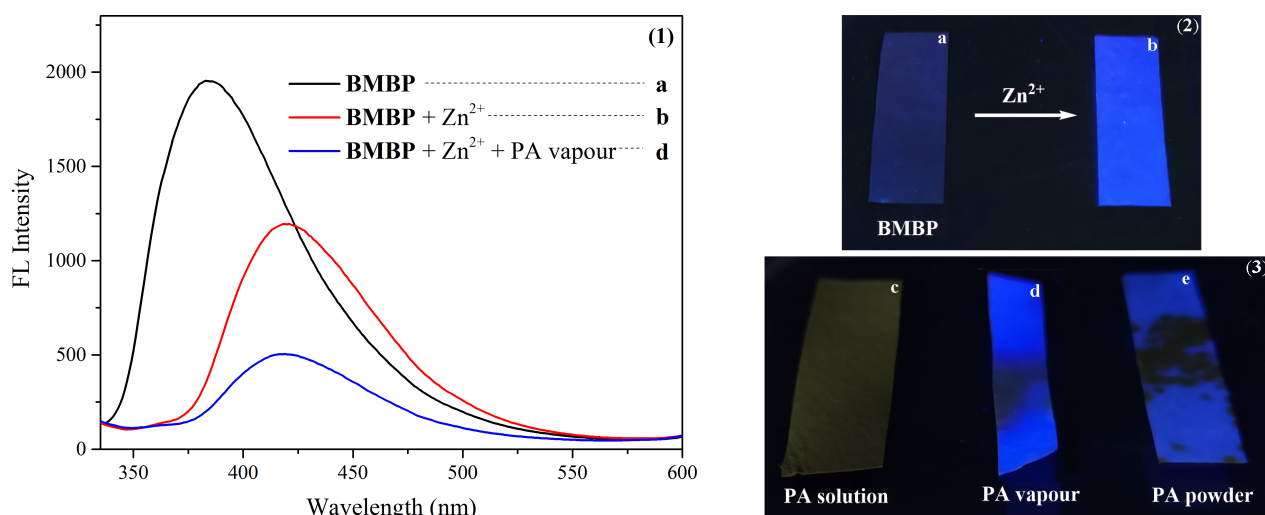


Fig. 12. (1): Fluorescence spectra of **BMBP**-coated test strips before (a) and after dropping with Zn^{2+} solution (b) and sequential fuming by PA vapour (d); (2)&(3): Photographs of visible detection of **BMBP**-coated test strips towards Zn^{2+} and sequential detection of PA in different forms (c: dissolved in water, d: vapour, e: powder) under 365 nm UV light.

In addition, we used the **BMBP-Zn²⁺** coated paper strips to sequentially detect PA dissolved in water, PA vapour and PA powder. The results are shown in **Fig. 12(3)**. Obviously, dark area can be found in the place where the paper strips have been contacted to the PA solution (c), PA vapour (d) and powder (e), respectively. These note that detecting PA in multiple forms with the **BMBP-Zn²⁺** coated paper strips can be visualized. Of course, the fluorescence intensity of **BMBP-Zn²⁺** coated paper strip largely decreases, e.g. upon exposing in PA vapour, which is shown as the line d in **Fig. 12(1)**. Thus, the above studies support that this readily accessible **BMBP**-coated paper strip can be served to sequentially detect Zn^{2+} and PA as a promising sensing device.

4. Conclusions

In summary, we have successfully synthesized a water-soluble fluorescence sensor **BMBP** in concise two steps. This novel sensor displays an intriguing sequential fluorescence sensing from Zn^{2+} to PA in the same aqueous system, concomitantly with “off-on-off” visible fluorescence response. Besides, **BMBP** possesses good sensing performance toward Zn^{2+} and PA on sensitivity, selectivity (distinguished response from multitude of analogues and common analytes) and pH tolerability. Delightedly, **BMBP** is also achieved to the wide application of sequential detection for Zn^{2+} and PA not only in real water samples, but also on the versatile paper strip. Importantly, the cascade fluorescence sensing mechanism from activated ICT to IFE&PET has been unveiled with the aid of comprehensive studies, which provides a good guidance to the building strategy of fluorescence sensor for sequential detection of ions and small molecules.

Acknowledgements

We are grateful to the Guangdong Provincial Science and Technology Project (No. 2017A010103016), Guangzhou Science and Technology Project Scientific Special (General Items, No. 201607010251), Open Fund of the Key Laboratory of Functional Molecular Engineering of Guangdong Province in SCUT (2017kf01) and NSF of Guangdong Province (No. 2014A030313429) for financial support.

References

- [1] Maret W, Li Y. Coordination dynamics of zinc in proteins. *Chem. Rev.* 2009; 109: 4682-707.
- [2] Goldberg JM, Wang F, Sessler CD, Vogler NW, Zhang DY, Loucks WH, et al. Photo-activatable sensors for detecting mobile zinc. *J. Am. Chem. Soc.* 2018; 140: 2020-3.

- [3] Chen JB, Gaillardet J, Louvat P. Zinc isotopes in the seine river waters, France: A probe of anthropogenic contamination. *Environ. Sci. Technol.* 2008; 42: 6494-501.
- [4] Lee MH, Kim JS, Sessler JL. Small molecule-based ratiometric fluorescence probes for cations, anions, and biomolecules. *Chem. Soc. Rev.* 2015; 44: 4185-91.
- [5] Murugan SA, Vidhyalakshmi N, Ramesh U, Annaraj JA. Schiff's base receptor for red fluorescence live cell imaging of Zn^{2+} ions in zebrafish embryos and naked eye detection of Ni^{2+} ions for bio-analytical applications. *J. Mater. Chem. B* 2017; 5: 3195-200.
- [6] Li J, Chen YH, Chen TT, Qiang J, Zhang ZJ, Wei TW, et al. A benzothiazole-based fluorescent probe for efficient detection and discrimination of Zn^{2+} and Cd^{2+} , using cysteine as an auxiliary reagent. *Sens. Actuators B* 2018; 268: 446-55.
- [7] Yoon SA, Lee J, Lee MH. A ratiometric fluorescent probe for Zn^{2+} based on pyrene-appended naphthalimide-dipicolylamine. *Sens. Actuators B* 2018; 258: 50-5.
- [8] Erdemir S, Tabakci B. Highly sensitive fluorometric detection of Zn^{2+} ion by calix[4]arene derivative appended 4-biphenylcarbonitrile. *Dyes Pigm.* 2018; 151: 116-22.
- [9] Mandal T, Hossain A, Dhara A, Al Masum A, Konar S, Manna SK, et al Terpyridine derivatives as "turn-on" fluorescence chemosensors for the selective and sensitive detection of Zn^{2+} ions in solution and in live cells. *Photochem. Photobiol. Sci.* 2018; 17: 1068-74.
- [10] Hwang MS, Kim C. Fluorescent detection of Zn^{2+} and Cu^{2+} by a phenanthrene-based multi-functional chemosensor that acts as a basic pH indicator. *Inorg. Chim. Acta* 2018; 482: 375-83.
- [11] Findik M, Ucar A, Bingol H, Guler E, Ozcan E. Fluorogenic ferrocenyl Schiff base for Zn^{2+} and Cd^{2+} detection. *Res. Chem. Intermed.* 2017; 43: 401-12.
- [12] Sun XC, Wang Y, Lei Y. Fluorescence based explosive detection: from mechanisms to sensory materials. *Chem. Soc. Rev.* 2015; 44: 8019-61.
- [13] Kaur I, Sharma V, Mobin SM, Kaur P, Singh K. Excitation wavelength based reversible multicolour photoluminescence by a single chromophore upon aggregation: Detection of picric acid-application in bioimaging. *Sens. Actuators B* 2019; 281: 613-22.
- [14] Tanwar AS, Adil LR, Afroz MA, Iyer PK. Inner filter effect and resonance energy transfer based attogram level detection of nitroexplosive picric acid using dual emitting cationic conjugated polyfluorene. *ACS Sens.* 2018; 3: 1451-61.

- [15] Adil LR, Gopikrishna P, Iyer PK. Receptor-free detection of picric acid: A new structural approach for designing aggregation-induced emission probes. *ACS Appl. Mater. Interfaces* 2018; 10: 27260-8.
- [16] Jiang K, Luo S-H, Pang C-M, Wang B-W, Wu H-Q, Wang Z-Y. A functionalized fluorochrome based on quinoline-benzimidazole conjugate: From facile design to highly sensitive and selective sensing for picric acid. *Dyes Pigm.* 2019; 162: 367-76.
- [17] Wei W, Lu R-J, Tang S-Y, Liu X-Y. Highly cross-linked fluorescent poly(cyclotriphosphazene-*co*-curcumin) microspheres for the selective detection of picric acid in solution phase. *J. Mater. Chem. A* 2015; 3: 4604-11.
- [18] Jiang N, Li GF, Che WL, Zhu DX, Su ZM, Bryce MR. Polyurethane derivatives for highly sensitive and selective fluorescence detection of 2,4,6-trinitrophenol (TNP). *J. Mater. Chem. C* 2018; 6: 11287-91.
- [19] Ponnuvel K, Banupriya G, Padmini V. Highly efficient and selective detection of picric acid among othernitroaromatics by NIR fluorescent organic fluorophores. *Sens. Actuators B* 2016; 234: 34-45.
- [20] Asthana SK, Kumar A, Neeraj, Shweta, Hira SK, Manna PP, et al. Brightening quinoline-imines by Al³⁺ and subsequent quenching by PPI/PA in aqueous medium: synthesis, crystal structures, binding behavior, theoretical and cell imaging studies. *Inorg. Chem.* 2017; 56: 3315-23.
- [21] Bhalla V, Kaur S, Vij V, Kumar M. Mercury-modulated supramolecular assembly of a hexaphenylbenzene derivative for selective detection of picric acid. *Inorg. Chem.* 2013; 52: 4860-5.
- [22] Santra DC, Bera MK, Sukul PK, Malik S. Charge-transfer-induced fluorescence quenching of anthracene derivatives and selective detection of picric acid. *Chem. - Eur. J.* 2016; 22: 2012-9.
- [23] Gogoi B, Sarma NS. Curcumin-cysteine and curcumin-tryptophan conjugate as fluorescence turn on sensors for picric acid in aqueous media. *ACS Appl. Mater. Interfaces*, 2015; 7: 11195-202.
- [24] Sandhu S, Kumar R, Singh P, Kumar S. Impact of aggregation on fluorescence sensitivity of molecular probes towards nitroaromatic compounds. *J. Mater. Chem. C* 2016; 4: 3209-16.

- [25] Huynh T-P, Wojnarowicz A, Kelm A, Woznicki P, Borowicz P, Majka A, et al. Chemosensor for selective determination of 2,4,6-trinitrophenol using a custom designed imprinted polymer recognition unit cross-linked to a fluorophore transducer. *ACS Sens.* 2016; 1: 636-9.
- [26] Bandela AK, Bandaru S, Rao CP. A fluorescent 1,3-diaminonaphthalimide conjugate of calix[4]arene for sensitive and selective detection of trinitrophenol: spectroscopy, microscopy, and computational studies, and its applicability using cellulose strips. *Chem. - Eur. J.* 2015; 21: 13364-74.
- [27] Ma HW, He CY, Li XL, Ablikim O, Zhang ST, Zhang M. A fluorescent probe for TNP detection in aqueous solution based on joint properties of intramolecular charge transfer and aggregation-induced enhanced emission. *Sens. Actuators B* 2016; 230: 746-52.
- [28] Zhang CL, Zhang SM, Yan YH, Xia F, Huang A, Xian YZ. Highly fluorescent polyimide covalent organic nanosheets as sensing probes for the detection of 2,4,6-trinitrophenol. *ACS Appl. Mater. Interfaces* 2017; 9: 13415-21.
- [29] Maity S, Shyamal M, Das D, Maity A, Dey S, Misra A. Proton triggered emission and selective sensing of 2,4,6-trinitrophenol using a fluorescent hydrosol of 2-phenylquinoline. *New J. Chem.* 2018; 42: 1879-91.
- [30] Peng ZW, Yuan D, Jiang ZW, Li YF. Novel metal-organic gels of bis(benzimidazole)-based ligands with copper(II) for electrochemical selectively sensing of nitrite. *Electrochim. Acta* 2017; 238: 1-8.
- [31] Zeng LL, Chen Y, Huang HY, Wang JQ, Zhao DL, Ji LN, et al. Cyclometalated ruthenium(II) anthraquinone complexes exhibit strong anticancer activity in hypoxic tumor cells. *Chem. - Eur. J.* 2015; 21: 15308-19.
- [32] Esteghamat-Panah R, Hadadzadeh H, Farrokhpour H, Simpson J, Abdolmaleki A, Abyar F. Synthesis, structure, DNA/protein binding, and cytotoxic activity of a rhodium(III) complex with 2,6-bis(2-benzimidazolyl)pyridine. *Eur. J. Med. Chem.* 2017; 127: 958-71.
- [33] Zou TT, Lum CT, Chui SSY, Che CM. Gold(III) complexes containing *N*-heterocyclic carbene ligands: Thiol "switch-on" fluorescent probes and anti-cancer agents. *Angew. Chem., Int. Ed.* 2013; 52: 2930-3.
- [34] Kumar A, Chae SP. Fluorescence tunable thiophene-bis(benzimidazole)-based probes for

- cascade trace detection of Hg^{2+} and lysine: A molecular switch mimic. *Sens. Actuators B* 2019; 281: 933-44.
- [35] Sun MT, Yu H, Zhang K, Wang SH, Hayat T, Alsaedi A, et al. A palladacycle based fluorescence turn-on probe for sensitive detection of carbon monoxide. *ACS Sens.* 2018; 3: 285-9.
- [36] Peng P, Xiong J-F, Mo G-Z, Zheng J-L, Chen R-H, Chen X-Y, et al. A concise synthesis of benzimidazoles *via* the microwave-assisted one-pot batch reaction of amino acids up to a 10-g scale. *Amino Acids* 2014; 46: 2427-33.
- [37] Rajnák C, Titiš J, Fuhr O, Ruben M, Boča R. Low spin Fe(II) complexes formed of mono-substituted 2,6-bis(2-benzimidazolyl)pyridine ligands. *Polyhedron* 2017; 123: 122-31.
- [38] Siddappa C, Kambappa V, Siddegowda AKC, Rangappa KS. One-pot synthesis of benzimidazoles from gem-dibromomethylarenes using *o*-diaminoarenes. *Tetrahedron Lett.* 2010; 51: 6493-7.
- [39] Wu Y-C, Jiang K, Luo S-H, Cao L, Wu H-Q, Wang Z-Y. Novel dual-functional fluorescent sensors based on bis(5,6-dimethylbenzimidazole) derivatives for distinguishing of Ag^+ and Fe^{3+} in semi-aqueous medium. *Spectrochim. Acta, Part A* 2019; 206: 632-41.
- [40] Zhang Y-Y, Chen X-Z, Liu X-Y, Wang M, Liu J-J, Gao G, et al. A highly sensitive multifunctional sensor based on phenylene-acetylene for colourimetric detection of Fe^{2+} and ratiometric fluorescent detection of Cd^{2+} and Zn^{2+} . *Sens. Actuators B* 2018; 273: 1077-84.
- [41] Wang LY, Cui MM, Tang H, Cao DR. Fluorescent nanoaggregates of quinoxaline derivatives for highly efficient and selective sensing of trace picric acid. *Dyes Pigm.* 2018; 155: 107-13.
- [42] Gao TB, Zhang JJ, Yan RQ, Cao DK, Jiang DC, Ye DJ. Aggregation-induced electrochemiluminescence from a cyclometalated iridium(III) complex. *Inorg. Chem.* 2018; 57: 4310-6.
- [43] Laschuk NO, Ebralidze II, Poisson J, Egan JG, Quaranta S, Allan JTS, et al. Ligand impact on monolayer electrochromic material properties. *ACS Appl. Mater. Interfaces* 2018; 10: 35334-43.
- [44] Ge YQ, Wei P, Wang T, Cao XQ, Zhang DS, Li FY. A simple fluorescent probe for monitoring pH in cells based on new fluorophore pyrido[1,2-a]benzimidazole. *Sens.*

Actuators B 2018; 254: 314-20.

- [45] Erdemir S, Kocyigit O. A novel dye based on phenolphthalein-fluorescein as a fluorescent probe for the dual-channel detection of Hg^{2+} and Zn^{2+} . *Dyes Pigm.* 2017; 145: 72-9.
- [46] Behera N, Manivannan V. A probe for multi detection of Al^{3+} , Zn^{2+} and Cd^{2+} ions *via* turn-on fluorescence responses. *J. Photochem. Photobiol. A* 2018; 353: 77-85.
- [47] Yao K, Fu J, Chang Y, Li B, Yang L, Xu K. A selective fluorescent probe for relay detection of Zn^{2+} and tartrate: Application to logic circuit and living cell imaging. *Spectrochim. Acta, Part A* 2018; 205: 410-8.
- [48] Kang JH, Han J, Lee H, Lim HM, Kim K-T, Kim C. A water-soluble fluorescence chemosensor for the sequential detection of Zn^{2+} and pyrophosphate in living cells and zebrafish. *Dyes Pigm.* 2018; 152: 131-8.
- [49] Fang L, Trigiante G, Kousseff CJ, Crespo-Otero R, Philpott MP, Watkinson M. Biotin-tagged fluorescent sensor to visualize 'mobile' Zn^{2+} in cancer cells. *Chem. Commun.* 2018; 54: 9619-22.
- [50] Kumar RS, Kumar SKA, Vijayakrishna K, Sivaramakrishna A, Paira P, Rao CVSB, et al. Bipyridine bisphosphonate-based fluorescent optical sensor and optode for selective detection of Zn^{2+} ions and its applications. *New J. Chem.* 2018; 42: 8494-502.
- [51] Dong W-K, Akogun FS, Zhang Y, Sun Y-X, Dong XY. A reversible "turn-on" fluorescent sensor for selective detection of Zn^{2+} . *Sens. Actuators B* 2017; 238: 723-34.
- [52] Jung JM, Kang JH, Han J, Lee H, Lim MH, Kim KT, et al. A novel "off-on" type fluorescent chemosensor for detection of Zn^{2+} and its zinc complex for "on-off" fluorescent sensing of sulfide in aqueous solution, *in vitro* and *in vivo*. *Sens. Actuators B* 2018; 267: 58-69.
- [53] Tang YF, Huang Y, Lu LX, Wang C, Sun TM, Zhu JL, et al. Synthesis of a new pyrene-derived fluorescent probe for the detection of Zn^{2+} . *Tetrahedron Lett.* 2018; 59: 3916-22.
- [54] Dong YW, Fan RQ, Chen W, Wang P, Yang YL. A simple quinolone Schiff-base containing CHEF based fluorescence 'turn-on' chemosensor for distinguishing Zn^{2+} and Hg^{2+} with high sensitivity, selectivity and reversibility. *Dalton Trans.* 2017; 46: 6769-75.
- [55] Wang FF, Zhang CF, Xue Q, Li HP, Xian YZ. Label-free upconversion nanoparticles-based fluorescent probes for sequential sensing of Cu^{2+} , pyrophosphate and alkaline phosphatase activity. *Biosens. Bioelectron.* 2017; 95: 21-6.

- [56] Kang JH, Lee SY, Ahn HM, Kim C. A novel colorimetric chemosensor for the sequential detection of Ni^{2+} and CN^- in aqueous solution. *Sens. Actuators B* 2017; 242: 25-34.
- [57] He LW, Yang XL, Xu KX, Kong XQ, Lin WY. A multi-signal fluorescent probe for simultaneously distinguishing and sequentially sensing cysteine/homocysteine, glutathione, and hydrogen sulfide in living cells. *Chem. Sci.* 2017; 8: 6257-65.
- [58] Li J, Yang C, Wang WL, Yan XP. Functionalized gold and persistent luminescence nanoparticle-based ratiometric absorption and TR-FRET nanoplatfrom for high-throughput sequential detection of L-cysteine and insulin. *Nanoscale* 2018; 10: 14931-7.
- [59] Kowser Z, Rayhan U, Rahman S, Georghiou PE, Yamato T. A fluorescence “turn-on” sensor for multiple analytes: OAc^- and F^- triggered fluorogenic detection of Zn^{2+} in a co-operative fashion. *Tetrahedron* 2017; 73: 5418-24.
- [60] Chandra R, Ghorai A, Patra GK. A simple benzildihydrazone derived colorimetric and fluorescent ‘on-off-on’ sensor for sequential detection of copper(II) and cyanide ions in aqueous solution. *Sens. Actuators B* 2018; 255: 701-11.
- [61] Sako AVF, Spudeit DA, Dupim M, Filho WPO, Saint’Pierre TD, de Oliveira MAL, et al. Dual-opposite end multiple injection method applied to sequential determination of Na^+ , K^+ , Ca^{2+} , Mg^{2+} ions and free and total glycerol in biodiesel by capillary zone electro-phoresis. *J. Chromatogr. A* 2018; 1570: 148-54.
- [62] Chang YX, Fu JX, Yao K, Li B, Xu KX, Pang XB. Novel fluorescent probes for sequential detection of Cu^{2+} and citrate anion and application in living cell imaging. *Dyes Pigm.* 2019; 161: 331-40.
- [63] Pandith A, Bhattarai KR, Siddappa RKG, Chae HJ, Seo YJ. Novel fluorescent C_2 -symmetric sequential *on-off-on* switch for Cu^{2+} and pyrophosphate and its application in monitoring of endogenous alkaline phosphatase activity. *Sens. Actuators B* 2019; 282: 730-42.
- [64] Ding JW, Yu NN, Wang XD, Qin W. Sequential and selective detection of two molecules with a single solid-contact chronopotentiometric ion-selective electrode. *Anal. Chem.* 2018; 90: 1734-9.
- [65] Hu YS, Kang J, Zhou PP, Han X, Sun JY, Liu SD, et al. A selective colorimetric and red-emitting fluorometric probe for sequential detection of Cu^{2+} and H_2S . *Sens. Actuators B* 2018; 255: 3155-62.

- [66] Ding AX, Shi YD, Zhang KX, Sun W, Tan ZL, Lu ZL, et al. Self-assembled aggregation-induced emission micelle (AIE micelle) as interfacial fluorescence probe for sequential recognition of Cu^{2+} and ATP in water. *Sens. Actuators B* 2018; 255: 440-7.
- [67] He L, Tao H, Koo S, Chen G, Sharma A, Chen Y, et al. Multifunctional fluorescent nanoprobe for sequential detections of Hg^{2+} ions and biothiols in live cells. *ACS Appl. Bio Mater.* 2018; 1: 871-8.
- [68] Malik AH, Hussain S, Kalita A, Iyer PK. Conjugated polymer nanoparticles for the amplified detection of nitro-explosive picric acid on multiple platforms. *ACS Appl. Mater. Interfaces* 2015; 7: 26968-76.
- [69] Pinrat O, Boonkitpatarakul K, Paisuwan W, Sukwattanasinitt M, Ajavakom A. Glucopyranosyl-1,4-dihydropyridine as a new fluorescent chemosensor for selective detection of 2,4,6-trinitrophenol. *Analyst* 2015; 140: 1886-93.
- [70] Yang G, Hu W-L, Xia H-Y, Zou G, Zhang Q-J. Highly selective and reproducible detection of picric acid in aqueous media, based on a polydiacetylene microtube optical waveguide. *J. Mater. Chem. A* 2014; 2: 15560-5.
- [71] Luo ZJ, Liu B, Si SF, Lin YJ, Luo CS, Pan CJ, et al. A fluorescent chemosensor based on nonplanar donor-acceptor structure for highly sensitive and selective detection of picric acid in water. *Dyes Pigm.* 2017; 143: 463-9.
- [72] Fu ZH, Wang YW, Peng Y. Two fluorescein-based chemosensors for the fast detection of 2,4,6-trinitrophenol (TNP) in water. *Chem. Commun.* 2017; 53: 10524-7.
- [73] Venkatesan N, Singh V, Rajakumar P, Mishra AK. Isobenzotriazolophanes: a new class of fluorescent cyclophanes as sensors for aromatic nitro explosives - picric acid. *RSC Adv.* 2014; 4: 53484-9.
- [74] Dey N, Samanta SK, Bhattacharya S. Selective and efficient detection of nitro-aromatic explosives in multiple media including water, micelles, organogel, and solid support. *ACS Appl. Mater. Interfaces* 2013; 5: 8394-400.
- [75] Tanwar AS, Hussain S, Malik AH, Afroz MA, Lyer PK. Inner filter effect based selective detection of nitroexplosive-picric acid in aqueous solution and solid support using conjugated polymer. *ACS Sens.* 2016; 1: 1070-7.
- [76] Liu SG, Luo D, Li N, Zhang W, Lei JL, Li NB, et al. Water-soluble nonconjugated polymer

- nanoparticles with strong fluorescence emission for selective and sensitive detection of nitro-explosive picric acid in aqueous medium. *ACS Appl. Mater. Interfaces* 2016; 8: 21700-9.
- [77] Luo TT, Li YQ, Xu YX, Zhang ST, Wang YJ, Kou XM, et al. Rapid synthesis of a hyper-fluorescence 2-pyridone derivative as a fluorescent molecular sensor for picric acid. *Sens. Actuators B* 2017; 253: 231-8.
- [78] Wang HP, Kang TT, Wang XJ, Feng LH. A facile strategy for achieving high selective Zn(II) fluorescence probe by regulating the solvent polarity. *Talanta* 2018; 184: 7-14.
- [79] Wang BJ, Dong WK, Zhang Y, Akogun SF. A novel relay-sensor for highly sensitive and selective detection of Zn^{2+}/Pic^- and fluorescence On/Off switch response of H^+/OH^- . *Sens. Actuators B* 2017; 247: 254-64.
- [80] Zhang ZY, Wang CJ, Zhang ZZ, Luo YJ, Sun SS, Zhang GQ. Cd(II) enhanced fluorescence and Zn(II) quenched fluorescence with phenylenevinylene terpyridine: A theoretical investigation. *Spectrochim. Acta, Part A* 2019; 209: 40-8.
- [81] Sit A, Giri D, Patra SK. Arylene-vinylene terpyridine conjugates: highly sensitive, reusable and simple fluorescent probes for the detection of nitroaromatics. *J. Mater. Chem. C* 2017; 5: 11100-10.
- [82] Yu XL, Wan JQ, Chen S, Li M, Gao JK, Yang L, et al. Pyridine-ring containing twisttetraaza- acene: Synthesis, physical properties, crystal structure and picric acid sensing. *Talanta* 2017; 174: 462-7.
- [83] Wu Y-C, Huo J-P, Cao L, Ding S, Wang L-Y, Cao DR, et al. Design and application of tri-benzimidazolyl star-shape molecules as fluorescent chemosensors for the fast-response detection of fluoride ion. *Sens. Actuators B* 2016; 237: 865-75.
- [84] Sarkar D, Pramanik A, Jana S, Karmakar P, Mondal TK. Quinoline based reversible fluorescent 'turn-on' chemosensor for the selective detection of Zn^{2+} : Application in living cell imaging and as INHIBIT logic gate. *Sens. Actuators B* 2015; 209: 138-46.
- [85] Dey N, Kulhanek J, Bures F, Bhattacharya S. Simultaneous detection of Cu^{2+} and Hg^{2+} via two mutually independent sensing pathways of biimidazole push-pull dye. *J. Org. Chem.* 2019; 84: 1787-96.

Highlights

- Concise design and synthesis of new fluorescence sensor with good water solubility.
- Sequential sensing from Zn^{2+} to PA with “off-on-off” response in water.
- Selective, sensitive and pH-tolerable sensing performance towards two analytes.
- Cascade mechanism revealed by MS, ^1H NMR, lifetime test and DFT calculation.
- Applicable in real water samples and paper strip for sequential detection.